Subwavelength Direct Laser Patterning of Conductive Gold Nanostructures by Simultaneous Photopolymerization and Photoreduction

Shobha Shukla,[†,⊥] Xavier Vidal,[⊥] Edward P. Furlani,[⊥] Mark T. Swihart,[§,⊥] Kyoung-Tae Kim,[†] Yong-Kyu Yoon,[†] Augustine Urbas,[∥] and Paras N. Prasad[†,‡,⊥,*]

[†]Department of Electrical Engineering, [‡]Department of Chemistry, [§]Department of Chemical and Biological Engineering, and [⊥]Institute for Lasers, Photonics and Biophotonics, University at Buffalo, State University of New York, Buffalo, New York 14260, United States, and [∥]Air Force Research Laboratory, Wright-Patterson Air Force Base, Ohio 45433, United States

ABSTRACT This article presents a new method for fabricating highly conductive gold nanostructures within a polymeric matrix with subwavelength resolution. The nanostructures are directly written in a gold precursor-doped photoresist using a femtosecond pulsed laser. The laser energy is absorbed by a two-photon dye, which induces simultaneous reduction of gold in the precursor and polymerization of the negative photoresist. This results in gold nanoparticle-doped polymeric lines that exhibit both plasmonic effects, due to the constituent gold nanoparticles, and relatively high conductivity (within an order of magnitude of the bulk metal), due to the high density of particles within these lines. Line widths from 150 to 1000 nm have been achieved with this method. Various optically functional structures have been prepared, and their structural and optical properties have been characterized. The influence of laser intensity and scan speed on feature size have been studied and found to be in agreement with predictions of a mathematical model of the process.

KEYWORDS: nanocomposites · two-photon lithography · metamaterials · gold nanostructures · nanofabrication

Fabrication of metallic nanostructures within a dielectric host material allows the optical response of the composite material to be tailored, potentially achieving responses not possible in a homogeneous material.[1−5] This capability is most notably exploited in the rapidly advancing field of optical metamaterials, a new class of nanostructured materials that exhibit electromagnetic properties, such as a negative refractive index, that are not observed in naturally occurring materials.[3,6−9] The unique properties of metamaterials arise from the engineered electromagnetic response of the constituent metallic nanostructures. Metamaterials hold promise for numerous applications such as far-field subwavelength imaging, invisibility cloaking, nanoscale optical trapping, ultracompact waveguides, and optical power limiting.[9−11] Most experimentally realized negative index metamaterials have been fabricated using "top-down" lithographic techniques, usually either electron-beam lithography (EBL) or focused-ion-beam lithography (FIBL).[1,3,8,12,13] Although these approaches can provide resolution on the scale of a few nanometers, they are inherently serial in nature and are limited to the fabrication of relatively small samples, typically with high-cost and low-throughput. A more recent approach to metamaterials involves direct laser writing in a polymeric structure followed by metal evaporation over the fabricated surface.[3] While this method is promising, full metal coverage is challenging. A need exists for new fabrication methods that overcome the aforementioned limitations.

In this paper we discuss, demonstrate, and analyze a novel bottom-up approach for the fabrication of conductive metal nano- and microstructures that is based on two-photon absorption-induced photochemistry.[14] This approach can significantly simplify the fabrication of metallic nanostructures in a polymeric host and can potentially enable fabrication of true three-dimensional metamaterials with low-cost and high-throughput. Although earlier studies have demonstrated the use of two-photon lithography to fabricate metallic micro- and nanostructures, most of this work has involved silver nanostructures, and very few prior studies investigated the use of gold.[15,16] The ability to write gold nanostructures in a polymeric host is not only useful for metamaterials but also has broader potential to enable disruptive advances in emerging fields such as flexible

*Address correspondence to pnprasad@buffalo.edu.

Received for review November 7, 2010 and accepted January 25, 2011.

Published online March 02, 2011
10.1021/nn103015g

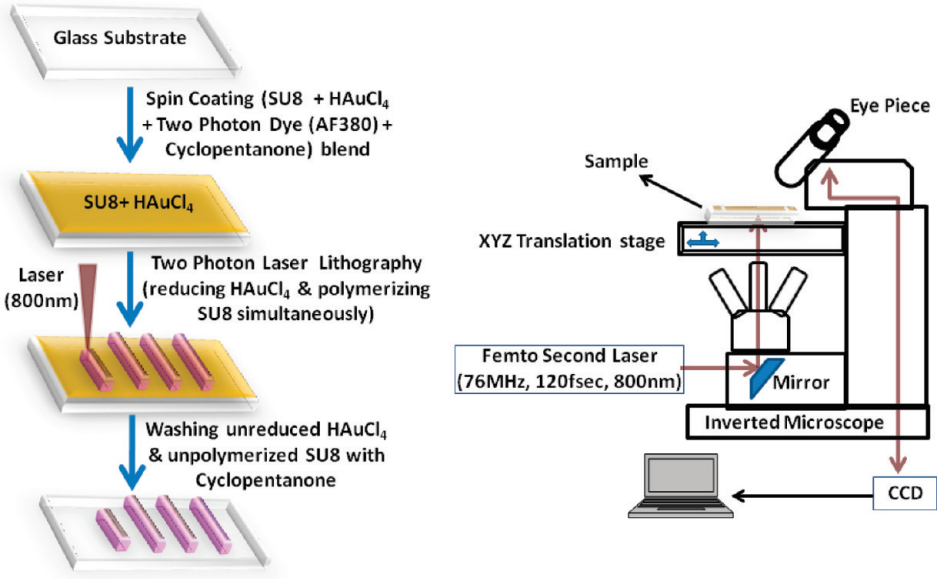

Figure 1. Schematic of the experimental setup.

electronics, nanophotonics, and plasmonics.[3,17−22]

Metallic structures can be directly written using the photoreduction of metal ions. Tanaka *et al.*[16] demonstrated the production of silver microstructures in an aqueous solution, but the reduced silver structures had non-uniform density due to diffusion and mixing effects that are driven by the femtosecond pulsed irradiation in the liquid. Baldacchini *et al.*[23] applied photoreduction of silver nitrate in a thin polymer (polyvinylpyrrolidone) film to produce metallic silver, and Maruo and Saeki[24] have adapted this process to write structures. However, this produced relatively low-quality metal structures due to discontinuities between aggregated nanoparticles. As noted above, there have been few reports on two-photon-assisted *in situ* photoreduction of gold ions.[15,16] Moreover, the methods reported so far not only suffer from diffusion and aggregation problems but also have been unable to achieve submicrometer feature sizes due to local heating during the writing process.

The two-photon-initiated direct laser writing method demonstrated and analyzed here is well-suited for the fabrication of micro- and nanoscale features because it is based on the initiation of a photochemical process within a small (subwavelength) focal volume that is limited in all three spatial dimensions.[1,14,25,26] Furthermore, simultaneous metal reduction and photopolymerization reduces diffusion-related broadening of features and nanoparticle aggregation because the matrix surrounding newly formed gold nanoparticles is cross-linked at the same time that the particles are formed. Thus, the metallic structures are simultaneously formed and immobilized. We demonstrate the use of this process for producing uniform gold nanoparticles within continuous gold nanoparticle-doped polymeric structures with line widths of 150 to 1000 nm. We also demonstrate production of optically functional structures and characterize these with respect to their structural, optical, and electrical properties (*i.e.*, conductivity). Our initial study suggests that even smaller line widths can be achieved using optimized combinations of laser and optics.

RESULTS AND DISCUSSION

The writing process is illustrated schematically in Figure 1 and described in greater detail in the Materials and Methods section. Typical directly written and developed metallic structures embedded in the polymer are shown in Figure 2. The SEM image (Figure 2a) illustrates the topography of the gold/polymer composite line, while the backscattered SEM in the lower right inset more clearly demonstrates the presence of gold nanoparticles within the polymer, based on the large atomic-number-based contrast difference between gold and the polymer. When the distance between two fabricated lines was small, some even smaller "bridging" structures were produced connecting the lines. This is similar to the effect observed by Tan *et al.*[27] and is attributed to the overlap of the low-intensity portion of the beam between the lines. Lines thus formed are a few hundred nanometers in width. By changing the laser power, we were able to tune the line width from 1 μm to as small as 150 nm, as shown in Figure 2b. SEM imaging of structures written at low laser power confirmed the production of polymeric lines as narrow as 150 nm, with gold nanoparticles ($\leq$50 nm diameter) embedded within them.

Cross-linked polymer lines containing gold nanoparticles can only be formed in the laser-exposed regions where the amount of photoacid generated is sufficient to both initiate polymerization of the SU8 monomer and reduce enough of the gold precursor to induce

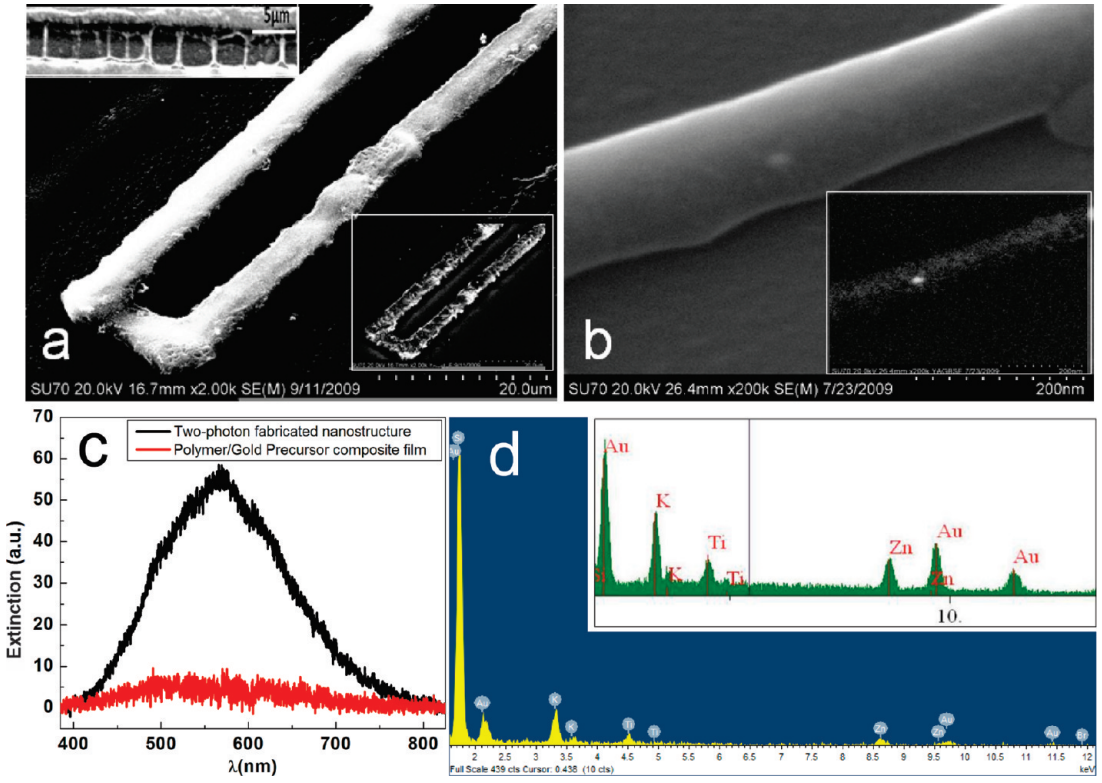

Figure 2. (a) Secondary electron emission image of the gold nanoparticle-doped polymeric structure produced at 50 mW laser power by two-photon-initiated photoreduction/polymerization (top inset, bridging structures formed when the spacing between the two lines was 4 μm; bottom inset, backscattered image showing gold nanoparticles). (b) Secondary emission SEM image of the structure fabricated at 20 mW laser power (inset: backscattered image). (c) Absorbance spectra of film with embedded gold nanostructures. (d) EDS spectra of the metallic structures.

particle nucleation. Normally, additional photoinitiator decomposition can occur by a free-radical driven cycle (*vide infra*). However, the gold precursor appears to compete with these reactions, decreasing the extent of photoinitiator decomposition. Thus, a relatively large amount of photoacid generator is required in this process. At low writing power (Figure 2b), the gold nanoparticles are concentrated near the center of the line, where the laser intensity is highest, while at an increased power of 50 mW, gold nanoparticles could be found throughout the fabricated structure (Figure 2a). As laser intensity increases, for a given exposure time, the width of the gold nanoparticle-rich region increases more than the width of the polymer line, showing that the photoreduction and photopolymerization have different threshold photon doses. Extinction spectra show a broad band centered at 570 nm (Figure 2c) that is attributed to excitation of localized surface plasmon resonances (LSPR) of the gold nanoparticles and that is not present in the unexposed film. Extinction spectra were recorded using a halogen lamp as a white light source and subtracting absorbance of the bare glass slide. The LSPR peak of gold nanoparticles can appear from 525 to 600 nm, depending on the size and shape of the nanoparticles and the coupling between them. In this sample, we have a distribution of nanoparticle sizes, and the particles are sufficiently close to one another to achieve overall conductivity. This broadens and red shifts the LSPR peak relative to that expected for small, monodispersed particles suspended in a solvent. Energy-dispersive X-ray spectroscopy (EDS) was also performed to check the composition of the fabricated structures (Figure 2d). The only elements detected were gold and the constituents of the glass substrate (*e.g.*, K, Zn, and Ti). The large peak from Si in the substrate is outside the energy range shown in the inset of Figure 2d. Notably, no chlorine is detected by EDS. This suggests that all gold in the lines is fully reduced, as one would expect that any ionic gold would be accompanied by chlorine counterions. For TEM imaging of gold nanoparticles produced within the polymeric matrix, the gold nanostructures were suspended in ethanol by scratching the fabricated polymeric gold composite structure with a diamond cutter tip and sonicating for 30 min. It is evident from TEM images, such as those shown in Figure 3, that the extracted gold nanoparticles are not aggregated and are highly crystalline. Figure 3a shows the crystallinity of individual nanoparticles, while Figure 3b–d shows gold nanoparticles still embedded in polymer. Of course, the sample of gold particles imaged in TEM is biased toward those that could be extracted from the film along with residual polymer. Perhaps these are particles near the edge of a line where both the density of

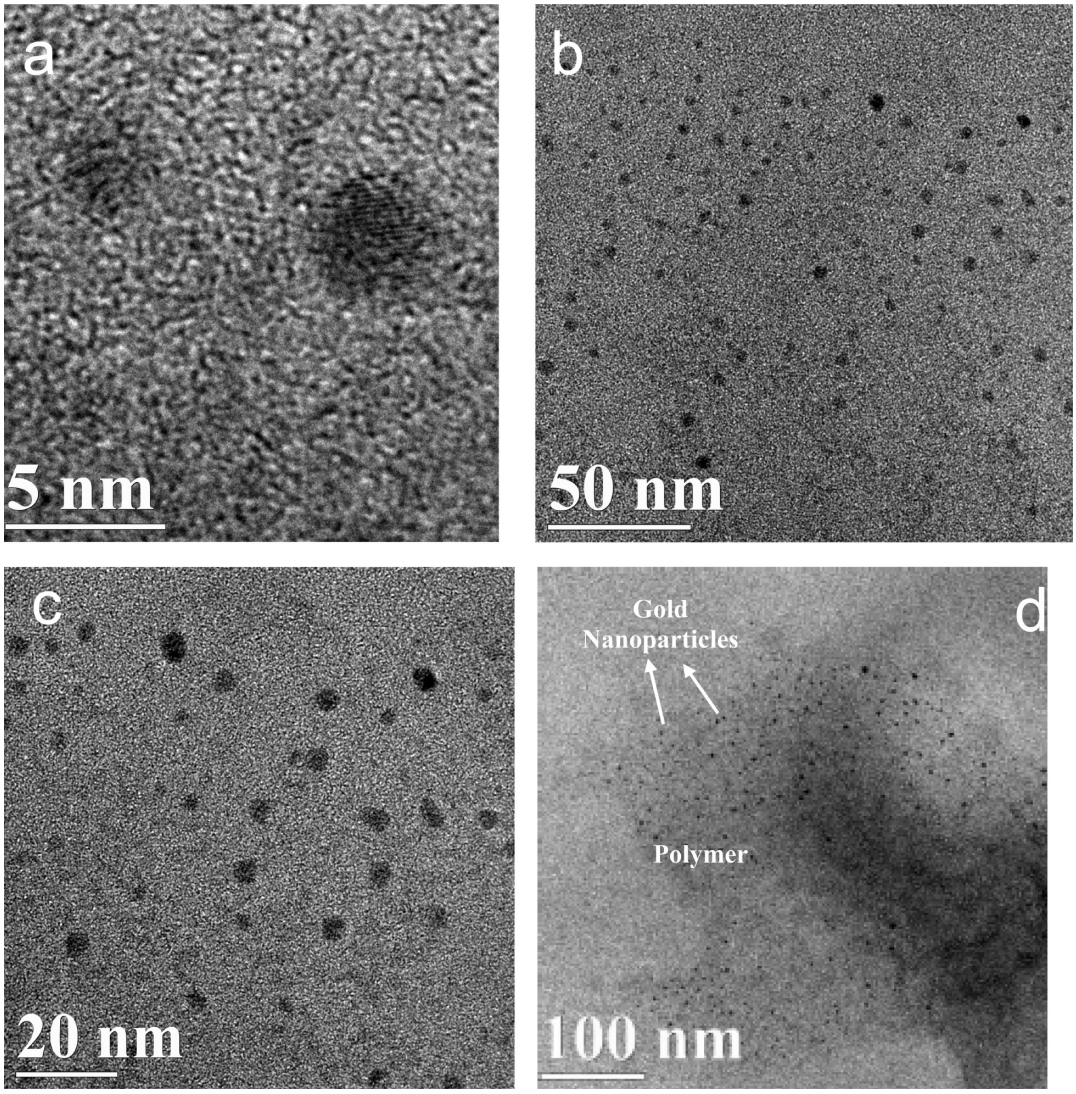

Figure 3. (a) High-resolution and (b−d) lower-resolution TEM images of gold nanoparticles extracted from fabricated structures.

gold and degree of SU8 cross-linking are lowest. Nonetheless, if the particles that can be extracted and imaged are fully reduced, crystalline gold, then any larger or partially sintered particles that remain in regions of higher photon dose should also be crystalline.

Laser-initiated photopolymerization of the SU8 oligomer with a photoacid generator is quite well understood, and metal photoreduction mechanisms have also been investigated recently.[27−32] The simultaneous photopolymerization and metal reduction has not been investigated, and specific mechanisms are unclear even in the case of laser-assisted metal reduction in a polymer matrix.[15,16,33] Nonetheless, we are able to infer a basic sequence of steps that must be involved. Hypothesizing such a series of steps for this complex process is a first step toward understanding it better. Thus we propose here a general mechanism for the simultaneous metal nanoparticle formation and photopolymerization. The precise mechanism may prove somewhat different, but full mechanistic understanding would require detection of intermediate species, which is beyond the scope of the present work. Mechanisms of energy transfer from a dye to other species, and of initiation of cationic polymerization in photolithography, can be found elsewhere.[13,24] Briefly, the two-photon dye absorbs energy at 800 nm and transfers energy to the photoacid generator. The excited photoacid generator decomposes, producing a strong acid, $HSbF_6$, which initiates cationic polymerization of SU8. We suggest that the photoinitiator (PC2506, a diaryliodonium salt photoacid generator, $Ar_2I^+SbF_6^-$), present in the SU8 film containing gold ions, is responsible for gold reduction as well as for cationic polymerization (cross-linking) of SU8.[29] When the photoinitiator oxidizes the SU8 monomer, either the (oxidized) SU8 monomer itself could reduce the gold ions, or organic free radical byproducts of photoacid generation could reduce the gold ion. The combined AF380-sensitized SU8 cross-linking and gold reduction are thus hypothesized to occur by a mechanism like that shown in Scheme 1.

Two-photon excitation of AF380:

$$AF380 + 2\,h\nu \longrightarrow AF380^{*} \quad (1)$$

Energy transfer to PC2506:

$$AF380^{*} + Ar_2ISbF_6 \longrightarrow AF380 + Ar_2ISbF_6^{*} \quad (2)$$

Aryl radical elimination from excited PC2506:

$$Ar_2ISbF_6^{*} \longrightarrow ArI{\bullet}SbF_6 + Ar{\bullet} \quad (3)$$

H-abstraction from monomer, polymer, or solvent:

$$ArI{\bullet}SbF_6 + RH \longrightarrow ArIHSbF_6 + R{\bullet} \quad (4)$$

Protonation of SU8 epoxy group by photoacid:

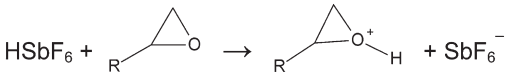

(5)

Cationic polymerization/crosslinking of SU8:

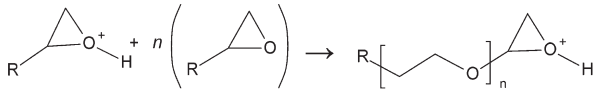

(6)

Hydrogen abstraction by aryl radical (or other radicals with the same effect):

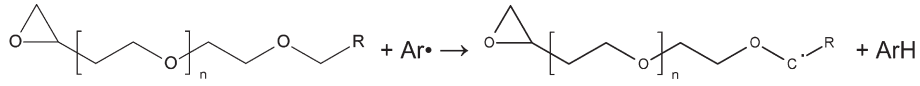

(7)

Gold reduction from Au^{3+} to Au^{2+} by SU8 radical:

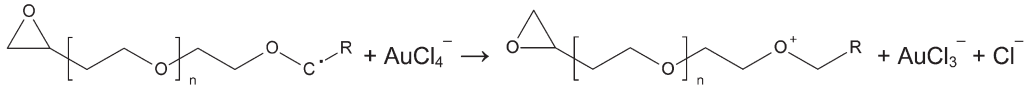

(8)

Fast disproportionation of Au^{2+}:

$$2\,AuCl_3^{-} \longrightarrow AuCl_2^{-} + AuCl_4^{-} \quad (9)$$

Disproportionation of Au^{1+} and Au^{2+} to produce Au^{3+} and Au^{0}:

$$AuCl_2^{-} + AuCl_3^{-} \longrightarrow AuCl_4^{-} + Au^{0} + Cl^{-} \quad (10)$$

Gold nanoparticle formation:

$$n\,Au^{0} \longrightarrow Au_n \quad (11)$$

Scheme 1. Proposed mechanism of simultaneous photoreduction and photopolymerization.

When photoacid, $HSbF_6$, is produced from the photoinitiator, aryl radicals and other radicals are produced as byproducts (Scheme 1, steps 3 and 4).[30] These can abstract hydrogen from the monomer or polymer to produce radicals by processes like that shown in step 7. In the absence of gold precursors, these radicals can react with the photoinitiator (step 8), leading to the cycle of free-radical-induced initiator decomposition shown in steps 7, 8, and 9 of Scheme 1.[30] In the presence of gold precursor, the radicals generated in step 7 may instead reduce the gold precursor as shown in step 10. The resulting $AuCl_3^{-}$ contains gold in the unstable Au^{2+} oxidation state. This undergoes disproportionation reactions like those illustrated in steps 11 and 12, ultimately producing one fully reduced Au^{0} atom for every three $AuCl_3^{-}$ ions generated by step 10 and regenerating two precursor ions ($AuCl_4^{-}$).[34−37] The Au^{0} atoms are expected to form gold nanoparticles by diffusion-limited aggregation. However, as they are produced, their mobility is also decreasing due to simultaneous cross-linking of SU8 in which they are formed. Of course, many minor variations of the above mechanism are conceivable, but a sequence of events like those listed here is consistent with the observed behavior of simultaneous photopolymerization and gold reduction and with known mechanisms of photopolymerization and gold reduction alone.

We have studied the effects of laser power and total photon dose on feature size by varying the scanning speed (Figure 4a) and the laser power. We were not able to use SEM imaging to compare line widths written at extremely low power, as these were easily washed off from the substrate during sample development. SEM imaging requires removal of the unexposed photoresist within which the lines are embedded. However, without the film for support, narrow lines often did not adhere to the substrate. Figure 2b shows a case where the polymerized line has remained on the substrate. However, in most other cases, the

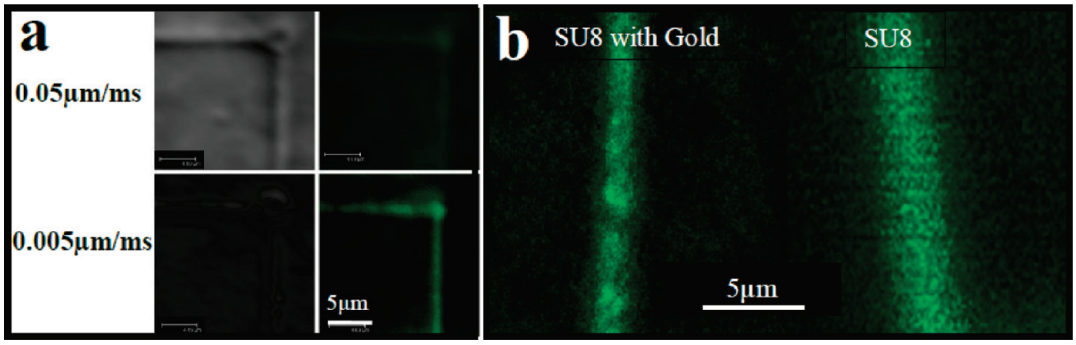

Figure 4. (a) Confocal transmission (left) and fluorescence (right) images of structures produced at scanning speeds of 50 μm s^{-1} (top) or 5 μm s^{-1} (bottom) at 10 mW. (b) Confocal images of gold precursor-doped polymeric feature and undoped polymeric feature at the same power (40 mW) and scan speed (50 μm s^{-1}).

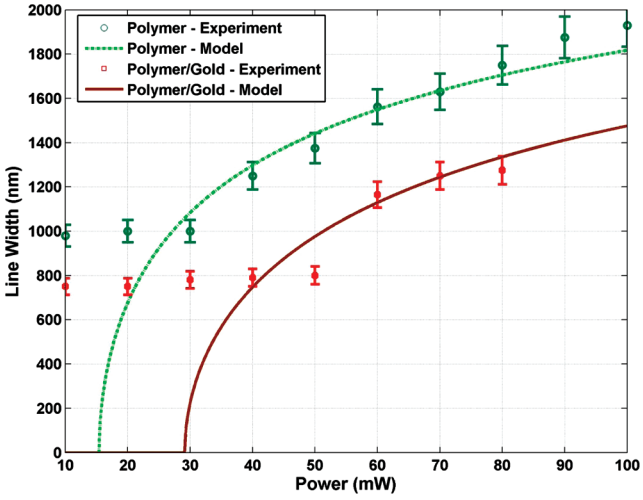

Figure 5. Polymerization line width *vs* laser power: comparison of model with experimental data.

lines were simply washed away, and a systematic study of the line width by SEM was not practical. Thus, for results shown in Figures 4 and 5, line widths were measured from confocal transmission images. With this approach, the apparent line width reflects both the writing resolution and the imaging resolution. This means that the apparent constant line width at low laser power may, in fact, reflect limitations of the line width measurement, which might be different for gold-containing lines *versus* gold-free lines because of the higher contrast between gold-containing lines and the surrounding matrix. In confocal fluorescence imaging, structures written at slower scan speeds showed brighter fluorescence but did not appear to be wider than those written at faster scan speeds (Figure 4a). However, this scan speed variation was only done with a relatively low power (~10 mW); at higher power, slow scan speeds led to ablation of the film. Formation of more pronounced features of the same apparent size at slower scan speeds could result from both a greater extent of gold reduction (producing more metallic gold which may increase dye emission *via* plasmonic field enhancement) and a higher degree of cross-linking (which would better trap the dye during postexposure washing). However, no detailed explanation can be confirmed at this time. In addition, we studied the influence of the gold precursor on the width of the feature size (Figure 4b). The minimum power required for producing a detectable polymeric feature, 10−15 mW, did not differ appreciably between SU8 alone and with the gold precursor added, but at higher power, this difference was more significant. The apparent width of the structure written at low power was ~750 nm for the gold-doped polymer sample and about 1000 nm for the undoped SU8. Confocal fluorescence images of the gold-doped polymer and undoped polymer at 40 mW are shown in Figure 4b, demonstrating a clear decrease in the apparent line width with the addition of gold precursor. In both cases, the observed feature width was independent of the laser power up to some threshold value (~30 mW for polymer alone and ~50 mW with gold precursor). Above that value, the line width increased with increasing laser power, as shown in Figure 5. We attribute the decrease in the line width and increase in the threshold for growth of line width to coupling between the photoinitiation of cationic polymerization and the gold reduction process.

We have developed a first-order analytical model to predict the line width w for our writing process. Following similar studies in the literature, we assume that SU8 is polymerized at positions where the total photoacid generated $\rho(x,y,z,t)$ exceeds a threshold value ρ_{th}. The equation governing the behavior of ρ is as follows

$$\frac{\partial \rho}{\partial t} = (\rho_0 - \rho)\sigma_{2,\,\mathrm{eff}} N^2 \tag{1}$$

where $\sigma_{2,\mathrm{eff}} = \sigma_2 \eta$ is the "effective" two-photon cross section, which is the product of the two-photon absorption coefficient, σ_2 (cm^4/s), of the dye used to sensitize the writing process (AF380) and the efficiency $\eta < 1$ of the initiation process. This efficiency represents the probability that excitation of the dye leads to energy transfer to the photoacid generator and production of the acid ($HSbF_6$ in this system). To the extent that the gold precursor ($AuCl_4^-$) can also participate in energy transfer from the dye and can react with (consume) the acid and free-radical byproducts of photoacid decomposition, this efficiency is expected to decrease with increasing concentration of the gold precursor. $N(x,y,z,t)$ is the photon flux. The laser output is defined by the wavelength λ of the incident light, the pulse repetition rate ν, the duration of the laser pulse τ_L during each repetition, and an average power P. We assume that N has a Gaussian spatial distribution at the focal plane ($z = 0$) and thus the photon flux at an observation point (x_{obs},y_{obs}) in this plane is

$$N(x, y, z = 0, t) = N_0(t)\exp\left[-2\frac{(x_b - x_{obs})^2 + (y_b - y_{obs})^2}{r_0^2}\right] \tag{2}$$

where (x_b,y_b) is the position of the center of the beam. We further assume that the photon flux is constant $N_0(t) = N_0$ during each pulse of duration τ_L. To determine the polymerized line width, we must account for the motion of the media during the writing process. To simplify the analysis, we choose a reference frame at rest with respect to the media and consider the laser beam to be moving along the y-axis with a constant velocity. The position of the center of the beam at time t is ($x_b = 0$, $y_b = v_b t$). We evaluate the polymerization at an observation point along the x-axis (x_{obs},$y_{obs} - 0$). Note that the beam will be over this point at $t = 0$ (*i.e.*, $y_b = y_{obs}$). We analyze an infinite scan line and integrate eq 1 as follows

$$\int_0^{\rho_a} \frac{d\rho}{(\rho_0 - \rho)} = \sigma_{2,\,\mathrm{eff}}\nu\tau_L N_0^2 \int_{-\infty}^{+\infty} \exp\left[-4\left(\frac{x_{obs}^2 + (v_b t)^2}{r_0^2}\right)\right] dt \tag{3}$$

where ρ_a is the density of activated photoacid generator. Note that to obtain eq 3 we have used the fact that the integrand is slowly varying during a laser pulse and that it decays exponentially with distance from the observation point. We set $\rho_a = \rho_{th}$ and solve eq 3 for x_{obs} to determine the distance $0 < x < x_{th}$ over which the film is polymerized. The polymerized line width $w = 2x_{th}$ is given by

$$w = r_0\left[\ln\left(\frac{\sqrt{\pi}\sigma_{2,\,\mathrm{eff}}\nu\tau_L r_0 N_0^2}{2v_b C}\right)\right]^{1/2} \tag{4}$$

where $C = \ln(\rho_0/(\rho_0 - \rho_{th}))$. In order to evaluate w we relate photon flux to the average laser power

$$N_0 = \frac{2}{\pi r_0^2 \nu\tau_L}\frac{TP}{\hbar\omega_L} \tag{5}$$

where T is the fraction of light transmitted through the objective. Finally, this leads to an overall expression for the line width:

$$w = r_0\left[\ln\left(\frac{\sigma_2\eta\left(\frac{TP}{\hbar\omega_L}\right)^2}{\pi^{3/2}v_b\nu\tau_L r_0^3 \ln\left(\frac{\rho_0}{\rho_0 - \rho_{th}}\right)}\right)\right]^{1/2} \tag{6}$$

All of the quantities in this expression are known or are readily measurable in separate experiments except for ρ_{th} and η. These can be fit to line width data. If the threshold photoacid concentration ρ_{th} is much smaller than the initial concentration ρ_0, then

$$C = \ln\left(\frac{\rho_0}{\rho_0 - \rho_{th}}\right) = \frac{\rho_{th}}{\rho_0} + \frac{1}{2}\left(\frac{\rho_{th}}{\rho_0}\right)^2 + \frac{1}{3}\left(\frac{\rho_{th}}{\rho_0}\right)^3 + \ldots \approx \frac{\rho_{th}}{\rho_0} \tag{7}$$

In this case, the expression for line width reduces to

$$w = r_0\left[\ln\left(\frac{\sigma_2\left(\frac{\eta\rho_0}{\rho_{th}}\right)\left(\frac{TP}{\hbar\omega_L}\right)^2}{\pi^{3/2}v_b\nu\tau_L r_0^3}\right)\right]^{1/2} \tag{8}$$

Under these conditions, the effects of ρ_{th} and η on the line width are indistinguishable. The effects could only be separated in experiments where the initial photoacid generator concentration, ρ_0, is not dramatically larger than the threshold photoacid concentration, ρ_{th}.

We apply eq 8 to our experimental results and model line width w as a function of laser power P for the two-photon-induced polymerization process, with and without the presence of the gold precursor. Results are shown in Figure 5. Our known experimental parameters are as follows: λ = 800 nm, v_b = 50 μm s^{-1}, τ_L = 120 fs, and ν = 76 MHz. The two-photon absorption cross section of the AF380 dye is $\sigma_2 = 3 \times 10^{-49}$ $\mathrm{cm}^4 \cdot$s. We fit eq 8 to our measured data, as shown in Figure 5,

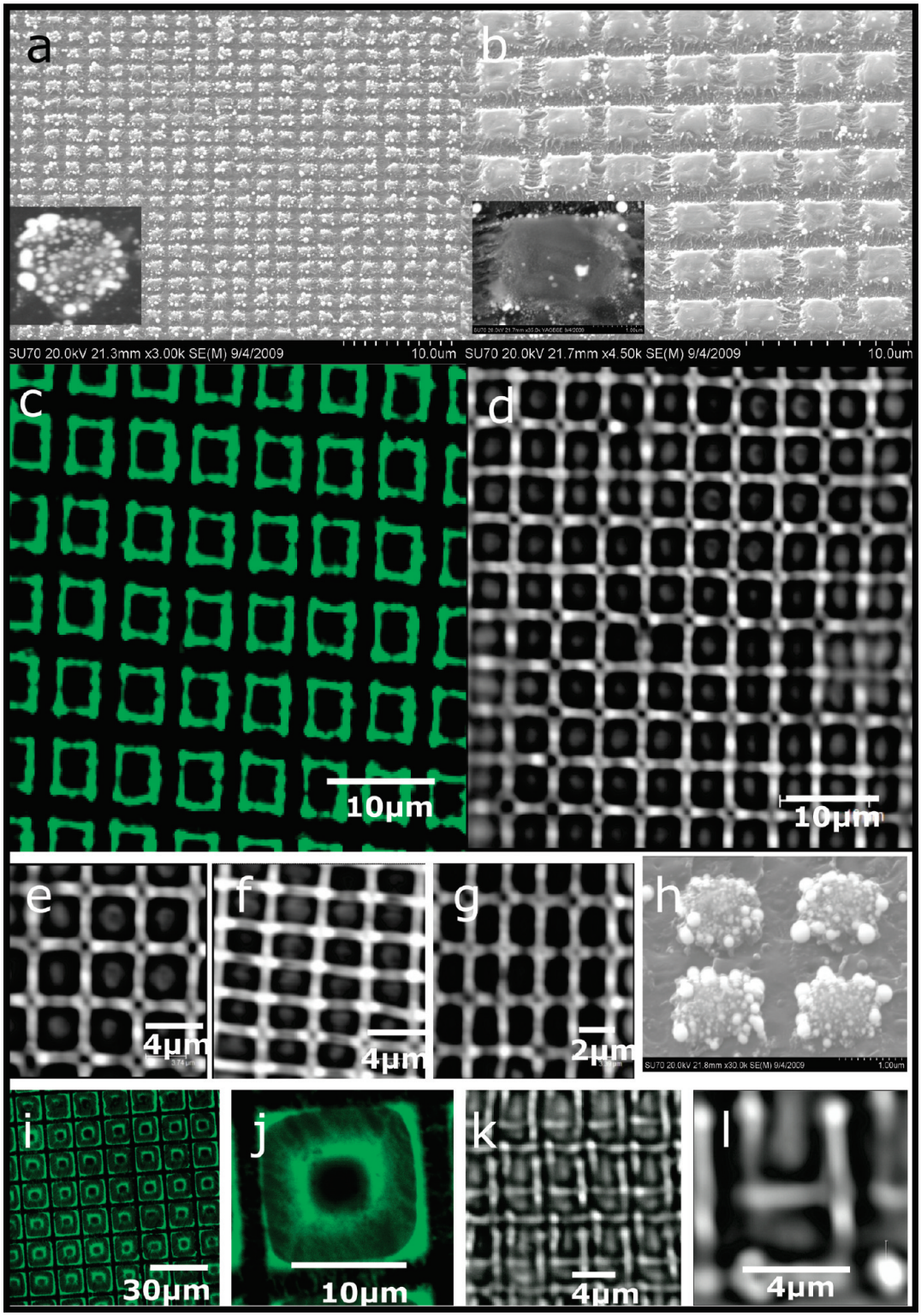

Figure 6. SEM image of (a) nanocauliflower; (b) nanoblocks (insets in a and b show the close-up view of the single element); (c) confocal fluorescence image of the SRR grating structure; (d) confocal transmission image of the fishnet structure; various structures made with femtosecond laser lithography: (e−g) fishnet structures, (h) plasmonic cauliflower, (i,j) plasmonic donuts; (k,l) chiral "y" structure.

using the following parameters: $r_0 = 940$ nm, $T = 30\%$, and $\eta\rho_0/\rho_{th} = 0.0028$ and 0.01 for polymerization with and without the gold precursor, respectively. The lower polymerization efficiency η in the presence of the gold precursor is due to the fact that it consumes products of photoacid decomposition, reducing the amount available for initiating cationic polymerization of SU8. These fits used only the data in the regime where line

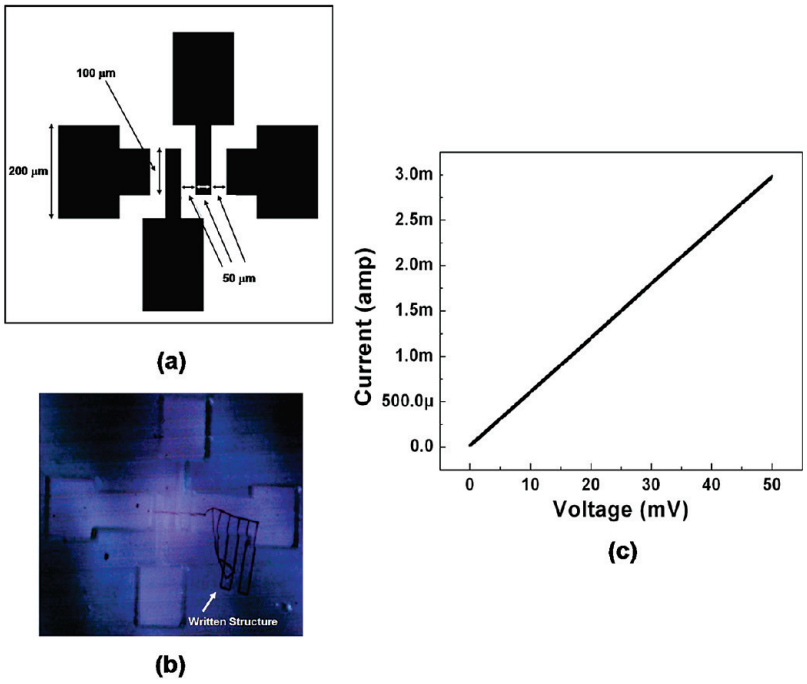

Figure 7. Electrical characterization of gold nanoparticle-doped line structure: (a) geometry of four-point probe measurement system; (b) four-point probe system; (c) current *vs* applied voltage.

width was observed to change with the laser power, which is where the line widths measured by confocal transmission microscopy are expected to be accurate. It is worth noting that extrapolating the polymer-only fit to a line width of zero gives a minimum laser power of 15 mW to produce any polymerization. This is consistent with the observed minimum energy required to produce an observable line. However, this experimental minimum energy for writing was not increased in the presence of gold precursor, in contrast to the prediction of this first-order model in which the gold precursor reduces the efficiency of photoacid generation independently of laser power. This suggests that the interaction between gold reduction and SU8 polymerization may be more complex than has been accounted for in this simple first-order model. Nonetheless, the model captures the experimental results with sufficient accuracy to serve as a useful guide to experiment. It should be noted that while we easily achieved subwavelength line width resolution with the gold precursor at low power, our optical system was not optimized to minimize the writing spot size. Therefore, a substantially finer writing resolution should be possible using the same process and materials with optimized optics and optomechanical components. As mentioned previously, periodically arranged metal nanostructures produce pronounced localized surface plasmon resonances, which result in an intense electromagnetic field that extends beyond their physical dimensions.[1,2,38−42] The nanostructures can support electric and magnetic resonances that give rise to resonant behavior of the effective bulk permittivity and permeability, respectively.[43,44] Figure 6a shows an electron micrograph of a gold "nano cauliflower" array. The diameter of the gold cauliflower element is 1 μm, and the periodicity is 2 μm. These structures were prepared using a high gold precursor loading (>30 wt %). The exact mechanism governing the formation of the structures is not presently understood and is a subject of our ongoing research. Metal nanoblocks made at comparatively higher power are shown in Figure 6b. The length to width ratio of these structures is 2.5 μm/1.5 μm, and the distance between two elements is approximately 4 μm. Split ring resonator (SRR) structures have also been prepared, as shown in Figure 6c. In these, the spacing between elements was 4 μm with an element height of 6 μm. The distance between the two ends of the split ring was kept at 2 μm. The most common approach to obtain a practical negative-index medium is through incorporation of nonmagnetic metallic resonators such as the split rings or various mesh (fishnet) structures. Figure 6d shows a gold wire mesh structure with a spacing of 5 μm between the neighboring wires. Several other structures prepared by two-photon lithography are shown in Figure 6e−l. In our preliminary report on this method, we also demonstrated production of chiral structures like those in Figure 6k,l, which calculations show can rotate the polarization of incoming light (also see Supporting Information S1).[10]

Last, we characterized the conductivity of the written lines. This is important because the level of conductivity of the fabricated structures will determine the range of utility of the writing process, especially as it

pertains to applications requiring functional electronic materials. We use a four-point probe approach to measure conductivity of individual lines, as illustrated in Figure 7a,b. The probe electrodes were deposited on prefabricated written structure on a glass substrate as shown in Figure 7b. The dimensions of the system are shown in Figure 7a. The conductivity measurement was performed using a digital source meter (Keithley 2400). Figure 7c shows the current *versus* applied voltage for a structure that was prepared with 30 wt % gold precursor loading. The fabricated gold lines were 800 nm wide and 300 μm long, and their conductivity ranged from 1 to 2.5 $\times$ 10^7 mho/m in various repeated experiments. Significantly, this is approximately 1/4 that of bulk gold, which is 4.1 $\times$ 10^7 mho/m. The relatively high conductivity of these structures is due to the high loading fraction of gold precursor and the photoreduction of the precursor into relatively small, densely packed gold nanoparticles. The ability to write subwavelength conductive structures that exhibit plasmonic effects is a significant and advantageous feature of the writing process and holds potential for numerous applications.

CONCLUSIONS

We have described, demonstrated, and analyzed a new laser-based direct writing method for producing subwavelength plasmonic and conductive patterned structures within a polymeric host. The method involves simultaneous two-photon-initiated photoreduction of a gold precursor and polymerization of a negative photoresist (SU8). Features with line widths as small as 150 nm have been produced using this approach. Several functional structures have been written including optically active planar chiral structures and plasmonic nanostructures, which are used in the development of composite metamaterials. We have studied various process parameters and have characterized their impact on the properties of fabricated structures. We expect this novel approach of *in situ* fabrication of plasmonic and conductive structures will enable efficient fabrication of novel three-dimensional optically functional composite media.

METHODS AND MATERIALS

The experimental arrangement for direct two-photon writing of gold nanostructures is shown schematically in Figure 1. SU8 (Microchem Inc.) served as the matrix within which gold structures were written by reduction of gold ions from $HAuCl_4$ incorporated within the unexposed SU8 film. SU8 includes a photoacid generator (PC2506, a diaryliodonium salt photoacid generator, $Ar_2I^+SbF_6^-$) as purchased. A two-photon dye, AF380 (provided by the US Air Force Research Laboratory, OH), was added to sensitize the mixture to two-photon absorption of infrared laser light. Composite films, typically containing 10 wt % gold precursor ($HAuCl_4 \cdot 3H_2O$, from Sigma Aldrich) and 1 wt % AF380 in the SU8 photoresist after solvent evaporation, were produced by spin-coating on glass coverslips. Cyclopentanone was used as a solvent for preparing the films because SU8, AF380, and $HAuCl_4$ are all highly soluble in it. The mixture was vortexed for 15 min and then ultrasonicated for 15 min to ensure complete dissolution and mixing.

Patterns were written within these films by irradiation with a mode-locked femtosecond pulsed laser (Ti:sapphire laser with an operating wavelength of 800 nm, a pulse width of <120 fs, and a repetition rate of 76 MHz). The laser light was introduced into an inverted microscope and focused with an air objective lens (60$\times$, NA0.85). The laser power was controlled by a graded neutral density filter. The laser power was measured at the entrance of the microscope; typical power loss from microscope entrance to the sample was approximately 25%. Unless otherwise indicated, a writing speed of 50 μm per second was used in the experiments reported here. After writing structures in the film, the unexposed portion could be removed by dipping the film in cyclopentanone and then allowing it to air-dry. No post-baking was performed; two-photon-initiated photopolymerization of SU8 can be done without post-baking because the temperature rise due to laser exposure at the focal region is sufficient to effectively anneal the focal volume.[45] Samples were studied using a confocal microscope (TCS SP2, Leica Microsystems Semiconductor GmbH) with an HXC PL APO CS 63.0 $\times$ 1.40 oil immersion objective. The samples were illuminated with a pulsed diode laser at 457 nm for fluorescence imaging of the patterned structure using the encapsulated dye. A photomultiplier tube (PMT) was used for detection, with a 480–580 nm band-pass filter for fluorescence and transmission imaging. For line width comparison experiments, the sample was post-baked for 2 min at 95 °C, developed with PGMEA, and washed with isopropyl alcohol (IPA) to make it photoinsensitive. With the inclusion of the gold precursor, the composite film cannot be fully washed with PGMEA and IPA as this will alter the patterned structure. Absorbance spectra of the fabricated structures were recorded with a UV–vis spectrophotometer (Ocean Optics Inc.). Energy-dispersive X-ray spectroscopy and scanning electron microscopy were performed using a Hitachi S-4000 field-emission SEM.

Acknowledgment. We thank Dr. A Baev and Dr. T Y Ohulchanskyy for helpful discussion. The support by Air Force office of Scientific Research (Grant No. FA95500910258) and National Science Foundation (CAREER 0748153) are also acknowledged.

Supporting Information Available: S1(a,b) Confocal image of the noncentrosymmetric structures: fluorescence and transmission image of (a) the left handed grating structure and (b) the right handed grating structure; (c) analysis of chiral gammadion structures: rotation of field polarization *vs* λ in the transmitted; scale bar = 2 μm; (d) computational model for a single element of a 2D array showing the presence of an E_y field component in the transmitted field. This material is available free of charge *via* the Internet at http://pubs.acs.org.

REFERENCES AND NOTES

1. Prasad, P. N. *Nanophotonics*; John Wiley & Sons: New York, 2004.
2. Oldenburg, S. J.; Averitt, R. D.; Westcott, S. L.; Halas, N. J. Nanoengineering of Optical Resonances. *Chem. Phys. Lett.* **1998,** *288*, 243–247.
3. Rill, M. S.; Plet, C.; Thiel, M.; Staude, I.; von Freymann, G.; Linden, S.; Wegener, M. Photonic Metamaterials by Direct Laser Writing and Silver Chemical Vapour Deposition. *Nat. Mater.* **2008,** *7*, 543–546.
4. Shukla, S.; Kumar, R.; Baev, A.; Gomes, A. S. L.; Prasad, P. N. Control of Spontaneous Emission of CdSe Nanorods in a Multirefringent Triangular Lattice Photonic Crystal. *J. Phys. Chem. Lett.* **2010,** *1*, 1437–1441.

5. Shukla, S.; Baev, A.; Jee, H.; Hu, R.; Burzynski, R.; Yoon, Y. K.; Prasad, P. N. Large Area near Infrared (IR) Photonic Crystals with Colloidal Gold Nanoparticles Embedding. *ACS Appl. Mater. Interfaces* **2010,** *2*, 1242–1246.
6. Smith, D. R.; Pendry, J. B.; Wiltshire, M. C. K. Metamaterials and Negative Refractive Index. *Science* **2004,** *305*, 788–792.
7. Shukla, S.; Kim, K.-T.; Baev, A.; Yoon, Y. K.; Litchinitser, N. M.; Prasad, P. N. Fabrication and Characterization of Gold−Polymer Nanocomposite Plasmonic Nanoarrays in a Porous Alumina Template. *ACS Nano* **2010,** *4*, 2249–2255.
8. Kuwata-Gonokami, M.; Saito, N.; Ino, Y.; Kauranen, M.; Jefimovs, K.; Vallius, T.; Turunen, J.; Svirko, Y. Giant Optical Activity in Quasi-Two-Dimensional Planar Nanostructures. *Phys. Rev. Lett.* **2005,** *95*, 227401–227404.
9. Furlani, E. P.; Baev, A. Optical Nanotrapping Using Cloaking Metamaterial. *Phys. Rev. E* **2009,** *79*, 026607–026612.
10. Baev, A.; Furlani, E. P.; Samoc, M.; Prasad, P. N. Negative Refractivity Assisted Optical Power Limiting. *J. Appl. Phys.* **2007,** *102*, 043101-5.
11. Furlani, E. P.; Baev, A. Free-Space Excitation of Resonant Cavities Formed from Cloaking Metamaterial. *J. Mod. Opt.* **2009,** *56*, 523–529.
12. Henzie, J.; Lee, J.; Lee, M. H.; Hasan, W.; Odom, T. W. Nanofabrication of Plasmonic Structures. *Annu. Rev. Phys. Chem.* **2009,** *60*, 147–165.
13. Lee, K. S.; Kim, R. H.; Yang, D. Y.; Park, S. H. Advances in 3D Nano/Microfabrication Using Two-Photon Initiated Polymerization. *Prog. Polym. Sci.* **2008,** *33*, 631–681.
14. Shukla, S.; Furlani, E. P.; Vidal, X.; Swihart, M. T.; Prasad, P. N. Two-Photon Lithography of Sub-Wavelength Metallic Structures in a Polymer Matrix. *Adv. Mater.* **2010,** *22*, 3695–3699.
15. Vurth, L.; Baldeck, P.; Stephan, O.; Vitrant, G. Two-Photon Induced Fabrication of Gold Microstructures in Polystyrene Sulfonate Thin Films Using a Ruthenium(II) Dye as Photoinitiator. *Appl. Phys. Lett.* **2008,** *92*, 171103-3.
16. Tanaka, T.; Ishikawa, A.; Kawata, S. Two-Photon-Induced Reduction of Metal Ions for Fabricating Three-Dimensional Electrically Conductive Metallic Microstructure. *Appl. Phys. Lett.* **2006,** *88*, 081107-3.
17. Henzie, J.; Lee, M. H.; Odom, T. W. Multiscale Patterning of Plasmonic Metamaterials. *Nat. Nanotechnol.* **2007,** *2*, 549–554.
18. Wang, M. C. P.; Gates, B. D. Directed Assembly of Nanowires. *Mater Today* **2009,** *12*, 34–43.
19. Nagpal, P.; Lindquist, N. C.; Oh, S.-H.; Norris, D. J. Ultrasmooth Patterned Metals for Plasmonics and Metamaterials. *Science* **2009,** *325*, 594–597.
20. Wu, Z.; Nelson, R. L.; Haus, J. W.; Zhan, Q. Plasmonic Electro-Optic Modulator Design Using a Resonant Metal Grating. *Opt. Lett.* **2008,** *33*, 551–553.
21. Nam, S.; Jiang, X.; Xiong, Q.; Ham, D.; Lieber, C. M. Vertically Integrated, Three-Dimensional Nanowire Complementary Metal-Oxide-Semiconductor Circuits. *Proc. Natl. Acad. Sci. U.S.A.* **2009,** *106*, 21035–21038.
22. Bratkovsky, A.; Ponizovskaya, E.; Wang, S. Y.; Holmstrom, P.; Thylen, L.; Fu, Y.; Agren, H. A Metal-Wire/Quantum-Dot Composite Metamaterial with Negative Epsilon and Compensated Optical Loss. *Appl. Phys. Lett.* **2008,** *93*, 193106-3.
23. Baldacchini, T.; Pons, A.-C.; Pons, J.; LaFratta, C.; Fourkas, J.; Sun, Y.; Naughton, M. Multiphoton Laser Direct Writing of Two-Dimensional Silver Structures. *Opt. Express* **2005,** *13*, 1275–1280.
24. Maruo, S.; Saeki, T. Femtosecond Laser Direct Writing of Metallic Microstructures by Photoreduction of Silver Nitrate in a Polymer Matrix. *Opt. Express* **2008,** *16*, 1174–1179.
25. Guo, R.; Li, Z.; Jiang, Z.; Yuan, D.; Huang, W.; Xia, A. Log-Pile Photonic Crystal Fabricated by Two-Photon Photopolymerization. *J. Opt. A: Pure Appl. Opt.* **2005,** *7*, 396–399.
26. Agren, H. Modeling of Multi-Photon-Induced Photoluminescence from Organic Fluorophores and Metal-Coated Semiconductor Nanoparticles. *Int. Symp. Biophotonics, Nanophotonics Metamaterial* **2006,** 26–26.
27. Tan, D.; Li, Y.; Qi, F.; Yang, H.; Gong, Q.; Dong, X.; Duan, X. Reduction in Feature Size of Two-Photon Polymerization Using SCR500. *Appl. Phys. Lett.* **2007,** *90*, 071106-3.
28. Kumi, G.; Yanez, C. O.; Belfield, K. D.; Fourkas, J. T. High-Speed Multiphoton Absorption Polymerization: Fabrication of Microfluidic Channels with Arbitrary Cross-Sections and High Aspect Ratios. *Lab Chip* **2010,** *10*, 1057–1060.
29. Cho, J.-D.; Ju, H.-T.; Park, Y.-S.; Hong, J.-W. Kinetics of Cationic Photopolymerizations of UV-Curable Epoxy-Based SU8-Negative Photoresists with and without Silica Nanoparticles. *Macromol. Mater. Eng.* **2006,** *291*, 1155–1163.
30. Acosta Ortiz, R.; Cisneros, M. d. L. G.; García, G. A. Synthesis of Novel Highly Reactive Silicone-Epoxy Monomers for Cationic Photopolymerizations. *Polymer* **2005,** *46*, 10663–10671.
31. Torigoe, K.; Esumi, K. Preparation of Colloidal Gold by Photoreduction of Tetracyanoaurate(1-)-Cationic Surfactant Complexes. *Langmuir* **1992,** *8*, 59–63.
32. Eustis, S.; El-Sayed, M. A. Molecular Mechanism of the Photochemical Generation of Gold Nanoparticles in Ethylene Glycol: Support for the Disproportionation Mechanism. *J. Phys. Chem. B* **2006,** *110*, 14014–14019.
33. Bellec, M.; Royon, A.; Bousquet, B.; Bourhis, K.; Treguer, M.; Cardinal, T.; Richardson, M.; Canioni, L. Beat the Diffraction Limit in 3D Direct Laser Writing in Photosensitive Glass. *Opt. Express* **2009,** *17*, 10304–10318.
34. Eustis, S.; El Sayed, M. A. Molecular Mechanism of the Photochemical Generation of Gold Nanoparticles in Ethylene Glycol: Support for the Disproportionation Mechanism. *J. Phys. Chem. B* **2006,** *110*, 14014–14019.
35. Kubo, S.; Diaz, A.; Tang, Y.; Mayer, T. S.; Khoo, I. C.; Mallouk, T. E. Tunability of the Refractive Index of Gold Nanoparticle Dispersions. *Nano Lett.* **2007,** *7*, 3418–3423.
36. Koga, H.; Tokunaga, E.; Hidaka, M.; Umemura, Y.; Saito, T.; Isogai, A.; Kitaoka, T. Topochemical Synthesis and Catalysis of Metal Nanoparticles Exposed on Crystalline Cellulose Nanofibers. *Chem. Commun.* **2010,** *46*, 8567–8569.
37. Kawamura, G.; Sato, S.; Muto, H.; Sakai, M.; Lim, P. B.; Watanabe, K.; Inoue, M.; Matsuda, A. AgBr Nanocrystal-Dispersed Silsesquioxane-Titania Hybrid Films for Holographic Materials. *Mater. Lett.* **2010,** *64*, 2648–2651.
38. Wang, W.; Summers, C. J.; Wang, Z. L. Large-Scale Hexagonal-Patterned Growth of Aligned Zno Nanorods for Nano-Optoelectronics and Nanosensor Arrays. *Nano Lett.* **2004,** *4*, 423–426.
39. Chan, Y.-H.; Chen, J.; Wark, S. E.; Skiles, S. L.; Son, D. H.; Batteas, J. D. Using Patterned Arrays of Metal Nanoparticles To Probe Plasmon Enhanced Luminescence of CdSe Quantum Dots. *ACS Nano* **2009,** *3*, 1735–1744.
40. Losic, D.; Shapter, J. G.; Mitchell, J. G.; Voelcker, N. H. Fabrication of Gold Nanorod Arrays by Templating from Porous Alumina. *Nanotechnology* **2005,** *16*, 2275–2281.
41. Veinot, J. G. C.; Yan, H.; Smith, S. M.; Cui, J.; Huang, Q.; Marks, T. J. Fabrication and Properties of Organic Light-Emitting Nanodiode Arrays. *Nano Lett.* **2002,** *2*, 333–335.
42. Lassiter, J. B.; Knight, M. W.; Mirin, N. A.; Halas, N. J. Reshaping the Plasmonic Properties of an Individual Nanoparticle. *Nano Lett.* **2009,** *9*, 4326–4332.
43. Lee, J. H.; Wu, Q.; Park, W. Metal Nanocluster Metamaterial Fabricated by the Colloidal Self-Assembly. *Opt. Lett.* **2009,** *34*, 443–445.
44. Bai, B.; Svirko, Y.; Turunen, J.; Vallius, T. Optical Activity in Planar Chiral Metamaterials: Theoretical Study. *Phys. Rev. A* **2007,** *76*, 023811–023823.
45. Seet, K. K.; Juodkazis, S.; Jarutis, V.; Misawa, H. Feature-Size Reduction of Photopolymerized Structures by Femtosecond Optical Curing of SU-8. *Appl. Phys. Lett.* **2006,** *89*, 024106-3.